

Knots and their effect on the tensile strength of lumber

Shuxian Fan

Department of Statistics, University of Washington

Samuel W K Wong

Department of Statistics and Actuarial Science, University of Waterloo

James V Zidek

Department of Statistics, University of British Columbia

March 16, 2022

Abstract

When assessing the strength of sawn lumber for use in engineering applications, the sizes and locations of knots are an important consideration. Knots are the most common visual characteristics of lumber, that result from the growth of tree branches. Large individual knots, as well as clusters of distinct knots, are known to have strength-reducing effects. However, industry grading rules that govern knots are informed by subjective judgment to some extent. Thus, the spatial interaction of knots and their relationship with lumber strength has not been fully understood. This paper reports the results of a study that investigated and modelled the strength-reducing effects of knots on a sample of Douglas Fir lumber. Experimental data were obtained by taking scans of lumber surfaces and applying tensile strength testing. The modelling approach presented incorporates all relevant knot information in a Bayesian framework, thereby contributing a more refined way of managing the quality of manufactured lumber.

Keywords: Bayesian predictive model; wood products; structural lumber testing; visual stress grading; strength-reducing characteristics; quality control

1 Introduction

This paper concerns a quality of sawn lumber known as its breaking strength, and how that strength is reduced by the presence of *knots*, i.e., defects in wood that result from the growth of tree branches. Due to the innate variability of lumber, methods for assessing its strength qualities are crucial to reduce consumer risk and ensure the safety of wood-based structures. The use of lumber as a construction material predates written history (Tegel et al., 2012). In Canada and the United States, its production grew rapidly around the turn of the 20th century (Reynolds and Pierson, 1923), establishing lumber as a major industry. More recently, the interest in wood as a sustainable material has led to the rise of mass timber structures (Harte, 2017).

Like any other manufactured product, lumber producers must monitor and ensure its quality. Although quality could be defined by a variety of criteria, the importance of any given criterion will be determined by consumers according to their intended application. For example wane, which is the presence of bark, may devalue a piece of lumber where aesthetics are important. But in construction and load-bearing applications, strength is the most important measure of lumber quality. The need to specify quality at the time of manufacture leads to a trade-off between producer risk (e.g., underestimating the lumber’s strength and value) and consumer risk (e.g., selecting lumber that fails to meet the strength requirements when placed in service). The idea of balancing these risks was recognized at least as far back as 1924, when rules were first established for sorting lumber into grades (Canadian Lumber Standards Accreditation Board, 2021).

The earliest grading rules were based on testing “clear” lumber specimens that were free of defects. Beginning in 1970, efforts to establish finer subdivisions of grades culminated in a large experiment in North America involving 70,000 pieces of sawn lumber, sampled from numerous mills in Canada and the United States (e.g., see Zidek and Lum, 2018, for a review). This led to the creation of grading rules that also incorporated visual characteristics or defects, such as knots, that were deemed to be strength-reducing. For example, these rules would specify the allowable sizes and locations of knots for a given grade, to help control the grade’s strength variation. Based on the experimental data, characteristic strength values (e.g., 5th percentile of the strength distribution) were estimated for the different grades, from which engineering design values (DVs) were subsequently derived. Consumers could then reasonably assume the strength of a random piece of lumber drawn from a given grade would lie above its published DV. This uniform system of assigning DVs underlies lumber manufacturing as we know it today.

The famous so-called “in-grade” experiment described above could be thought of as a process capability analysis, in the terminology of modern quality control theory. Like any other process, it was anticipated that the DVs might decline due to assignable causes such as climate change or insect infestation. As a result, monitoring programs were established for North American lumber to detect changes to strength properties within grades (Kretschmann et al., 1999). If significant changes were to occur, updates to DVs or grading rules would be needed. Since visual characteristics are a key component of grading rules, understanding their relationship with strength is an important research problem.

The use of visual characteristics to predict lumber strength is well-established in the literature. For example, in so-called weak zone models, each piece of dimensional lumber is conceptualized as a composite of clear wood sections connected by weak sections, where the location of lumber defects can vary randomly (Kandler et al., 2015; García and Rosales,

2017). In the lumber tensile strength models proposed by Taylor et al. (1992), a piece of lumber is similarly considered to be comprised of smaller contiguous segments. Regression methods have also been used to predict lumber strength based on associated characteristics, such as knot area ratios and the maximum diameters of the estimated strength-reducing knots (Divos and Tanaka, 1997; França et al., 2018). The efficacy of applying modern statistical methods for grading design purposes has also been established, as in a recent study by Wong et al. (2016). That work proposed a Bayesian approach for constructing a coherent hierarchical framework for modelling lumber strength, based on the characteristics recorded from the grading process and the uncertainties involved. Visual characteristics were recorded in accordance with grading rules, which included the knot deemed to be the most strength-reducing, the presence or absence of shake (a separation of lumber along its grain), and a miscellaneous category to cover other defects.

Knots, formed from branches or limbs during the growth of the tree, constitute the most important strength-reducing characteristic of dimensional lumber (Foley, 2003). Sawing practices result in *knot faces* visible on lumber surfaces as dark elliptical cross-sections that cause fibre distortion. Clusters of knots, as well as other knots in close proximity, are known to have combined effects in reducing the strength of lumber (Oh et al., 2010; Fink and Kohler, 2014). However, grading rules only require the details for a single knot (or knot cluster) to be recorded, and selecting that maximum strength-reducing knot requires some subjective judgment. Due to these grading limitations, the complete spatial arrangement of knots has not been used in previous strength prediction models for lumber specimens, to the best of our knowledge. Therefore, the spatial interaction of knots and their relationship with strength properties requires further study and model development.

While knots appear on the surfaces of sawn lumber as elliptical shapes, these knot faces are only cross-sections of their underlying three-dimensional (3-D) structure. The idea of exploiting 3-D knot information to inform the strength of lumber was shown to be promising in Lukacevic et al. (2015). To infer 3-D structure from the knot faces, a procedure known as *knot matching* can be applied to determine the likely correspondence between visible ellipses and tree branches (Jun et al., 2019). This then allows the 3-D structure and volume of each knot to be reconstructed, based on the knot faces that are matched together. We leverage these recent developments in this paper so that the strength-reducing effects of knots can be modelled as accurately as possible.

Given the above considerations, this paper proposes a new approach for modelling the tensile strength of lumber based on the observed spatial arrangement of knots and their inferred 3-D volumes. Rather than obtaining data from the grading process (e.g., as in Wong et al., 2016), this study extracts the full knot information directly from surface scans of specimens. We focus on tensile strength, which is measured by a destructive test that pulls longitudinally on the two ends of a piece of lumber until it breaks. Our model is designed to describe how the joint strength-reducing effects of knots vary longitudinally for individual lumber specimens. We adopt a Bayesian approach for inference, and demonstrate the efficacy of the proposed model via simulation studies and an analysis of experimental data collected from a sample of Douglas Fir specimens.

Our paper is laid out as follows. In Section 2, we propose our Bayesian model for lumber tensile strength and its inference. In Section 3, we use simulated data to illustrate that our proposed framework leads to well-behaved inference results. A description of the Douglas Fir experimental data, and the results of applying the proposed model to that dataset, are presented in Section 4. The predictive performance of the fitted model is also investigated

and compared to baseline regression models via cross-validation. We conclude the paper in Section 5 with a discussion of the insights gained into the joint strength-reducing effects of knots and the implications of this study for future work.

2 Framework for Modelling Lumber Strength

2.1 Model Conceptualization

For a given lumber specimen we will observe a collection of knots with various sizes and locations, and this section develops a framework for modelling the impact of the knots on tensile strength. To provide a realistic characterization of strength, the model should account for the recorded features of all strength-reducing knots, and other sources of uncertainty inherent to the specimen itself. To do so, we adopt a hierarchical structure that nests a process model (X) within a measurement model (Y).

The process model is conceptualized by considering a “clear” specimen with no knots, and the measurement model then adjusts for the strength-reducing effects of knots. The idea is to then partition the specimen longitudinally into adjacent rectangular cells, similar to the segmenting done in previous studies (Taylor et al., 1992). Figure 1 illustrates such a partitioning with J cells, where the knot faces from the surface of a sample specimen are visible. The number of cells J is chosen to reflect the highest resolution at which failure locations can be accurately determined from a tensile strength test; that is, after testing we can observe the failure to have occurred in cell $j \in \{1, 2, \dots, J\}$. Then, specifying the process model over each cell provides a discretized representation of how strength varies along the piece of lumber.

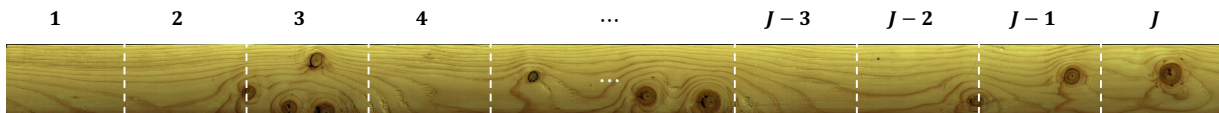


Figure 1: Partitioning a lumber specimen into J cells, using the surface of a sample specimen to illustrate. The dark elliptical shapes are the visible knot faces, and the cell boundaries are marked by the dotted lines. For example, there are four knot faces that are distinctly visible within cell 3.

Strength of a Clear Specimen

We define a “clear” specimen to be one that has no knots. Consequently, the within-specimen strength variability of a clear specimen arises from other uncertainties associated with destructive strength testing and potentially other strength-reducing characteristics apart from knots. We then assume the strength varies randomly along the length of a lumber specimen, with strengths of adjacent cells being autocorrelated.

Let the strength of the cells in a “clear” specimen be represented by the vector $\mathbf{X} = \{X_1, \dots, X_J\} \in \mathbb{R}^J$. We use an $AR(1)$ process of the form

$$X_j = \alpha + \rho X_{j-1} + \epsilon_j, \quad 0 < \rho < 1, \quad \epsilon_j \stackrel{iid}{\sim} N(0, \sigma^2), \quad j = 2, \dots, J$$

to model the autocorrelation among the X_j 's, where the mean is $\mu = E[X_j] = \alpha/(1 - \rho)$ for $j = 1, \dots, J$ and $X_1 \sim N(\mu, \sigma^2/(1 - \rho^2))$. Additional global or local covariates can be included in the framework by replacing α with a regression component $\boldsymbol{\eta}^T \mathbf{v}_j$, i.e.,

$$E[X_j | X_{j-1} = x_{j-1}, \mathbf{v}_j] = \rho x_{j-1} + \boldsymbol{\eta}^T \mathbf{v}_j, \quad (1)$$

where \mathbf{v}_j denotes the covariate vector for cell j and $\boldsymbol{\eta}$ is a vector of regression coefficients. If only global covariates (i.e., those common among all cells of the specimen) are used, then the $AR(1)$ process is stationary. Covariates could include any features of the specimen that can be measured non-destructively (i.e., without breaking the specimen) that are associated with strength.

Strength Adjusted for the Presence of Knots

Many previous studies have demonstrated the significant impact of knots, and the resulting fibre deviations, on the strength properties of dimensional lumber (Castéra et al., 1996; Cramer and Goodman, 1983; Hietaniemi and Silvén, 2011). In particular, knots that straddle the edge of a piece (or *edge knots* for short) are considered to have larger strength-reducing effects compared to other types of knots (Courchene et al., 1998). Therefore, it is important to consider both the overall spatial arrangement of knots and the placement of each individual knot within a specimen. For example, in the specimen shown in Figure 1, the bottom two knot faces visible in cell 3 are edge knots.

The number and location of knots on a specimen are random and might be conceptualized as a realization of a spatial point process. Here, we simply take their observed spatial arrangement as given, after extracting all relevant knot information from scans of the lumber surfaces. To be more precise, suppose a specimen has K knots, and let Z_k denote the intrinsic strength-reducing effect of the k -th knot, $k = 1, \dots, K$, which in this paper we take to be the 3-D volume displaced by the knot (Lukacevic et al., 2015). Then, we define the measurement model \mathbf{Y} to be the process model adjusted by the joint strength-reducing effects of all K knots. For a particular cell j , its adjusted strength Y_j will depend on knots within the cell, together with contributions from knots in other cells albeit to a lesser extent. Intuitively, the impact of a knot will decrease according to its relative distance from the cell.

Given the above considerations, we model Y_j with the form

$$Y_j = X_j - \sum_{k=1}^K \gamma_{(k)} h(d_{jk}) Z_k,$$

where d_{jk} is the distance between the centroids of knot k and cell j , and $h(d_{jk})$ is a decreasing function of d_{jk} . The coefficient $\gamma_{(k)}$ then scales these distance-weighted knot effects to a corresponding reduction in strength for the cell, defined according to

$$\gamma_{(k)} = \begin{cases} \gamma_0 & \text{if the } k^{\text{th}} \text{ knot is not an edge knot} \\ \gamma_1 & \text{if the } k^{\text{th}} \text{ knot is an edge knot.} \end{cases}$$

Observed Strength of a Specimen with Knots

Tensile strength testing applies loads uniformly across the length of the specimen, so that the specimen is expected to break at its weakest location. In our discretized representation

of strength along the specimen, the observed strength will thus be that of the weakest cell among the J cells, where the index of the cell corresponding to the location of failure is also observed. Specifically, the observed strength measurement Y_{obs} for the specimen is $Y_{obs} = Y_m$, where $m = \arg \min_j \{Y_j : j = 1, \dots, J\}$. This construction induces truncated distributions for the strengths in other cells, since $Y_j > Y_m$ for $j \neq m$.

2.2 Bayesian Inference

We adopt a Bayesian approach to infer the model parameters in the preceding framework, given the observed data from a sample of n specimens. This allows us to incorporate relevant prior information into the model and to obtain predictive distributions for the strengths of future specimens that coherently account for the posterior uncertainties of the parameters.

Considering specimen i of the sample, $i = 1, \dots, n$, let $K_i \geq 0$ be the number of knots in the specimen and $\mathbf{S}_i = [\mathbf{s}_1, \dots, \mathbf{s}_{K_i}]$ their corresponding knot centroids. Denote the centroids of the J cells in the partitioning by $[\mathbf{c}_1, \mathbf{c}_2, \dots, \mathbf{c}_J]$, then define the distance matrix $\mathbf{D}_i \in \mathbb{R}^{J \times K_i}$ as

$$\mathbf{D}_i = [\mathbf{d}_1, \mathbf{d}_2, \dots, \mathbf{d}_{J-1}, \mathbf{d}_J]^T,$$

where $\mathbf{d}_j = \|\mathbf{S}_i - \mathbf{c}_j\|_2 \in \mathbb{R}^{K_i}$ is the vector of Euclidean distances between the j -th cell and each knot. In this paper we use a simple exponential decay for the distance function, $h(d) = \exp\{-\beta d\} \mathbb{I}(d \leq d_{\max})$ where β is a parameter to be estimated and d_{\max} is the maximum distance at which a knot can have an impact on strength. Then the weight matrix $\mathbf{W}_i \in \mathbb{R}^{J \times K_i}$ is obtained by applying the function $h(\cdot)$ to \mathbf{D}_i element-wise. Finally, let $\mathbf{Z}_i \in \mathbb{R}^{K_i \times 1}$ denote the intrinsic strength-reducing effects of the K_i knots and $\mathbf{E}_i \in \{0, 1\}^{K_i \times 1}$ be a vector of indicators with 1 denoting an edge knot. All of K_i , \mathbf{D}_i , \mathbf{Z}_i , and \mathbf{E}_i will be observed for the specimen.

Next we turn to the strength model, and let $\mathbf{X}_i \in \mathbb{R}^{J \times 1}$ denote the strengths of the J cells when specimen i is clear of knots, assumed to follow an $AR(1)$ process and have a normal distribution as presented in Section 2.1. Taking the setup in Equation (1) where \mathbf{X}_i also depends on covariates, let \mathbf{v}_{ij} denote the relevant covariates for cell j and $\boldsymbol{\eta}$ the vector of coefficients. Then \mathbf{Y}_i is the vector of cell strengths adjusted for knots and given by

$$\mathbf{Y}_i = \mathbf{X}_i - \mathbf{W}_i \times (\{\gamma_0(\mathbf{1}_{K_i} - \mathbf{E}_i) + \gamma_1 \mathbf{E}_i\} \circ \mathbf{Z}_i), \quad (2)$$

where $\mathbf{1}_{K_i}$ is a column vector of K_i ones and \circ is the element-wise product. After the tensile test, denote the strength measurement observed for the specimen as $Y_{obs,i}$, which is defined by the minimum of the underlying adjusted strengths, i.e., $Y_{obs,i} = \min\{\mathbf{Y}_i\}$ and let m_i denote the corresponding cell index of the failure location.

Then the model parameters to be inferred from the sample are in vectorized form, $\boldsymbol{\theta} = [\boldsymbol{\eta}, \rho, \sigma^2, \beta, \gamma_0, \gamma_1]$, which has posterior distribution given by

$$\begin{aligned} p(\boldsymbol{\theta} | \{Y_{obs,i}, m_i, K_i, \mathbf{D}_i, \mathbf{Z}_i, \mathbf{E}_i\}_{i=1}^n) &\propto \pi(\boldsymbol{\theta}) \prod_{i=1}^n p(Y_{obs,i}, m_i | K_i, \mathbf{D}_i, \mathbf{Z}_i, \mathbf{E}_i, \boldsymbol{\theta}) \\ &\propto \pi(\boldsymbol{\theta}) \prod_{i=1}^n \int_A p(\mathbf{Y}_i | K_i, \mathbf{D}_i, \mathbf{Z}_i, \mathbf{E}_i, \boldsymbol{\theta}) d\mathbf{Y}_{-obs,i} \end{aligned} \quad (3)$$

where $\pi(\boldsymbol{\theta})$ denotes the joint prior distribution of the parameters, $\mathbf{Y}_{-obs,i}$ is \mathbf{Y}_i with element m_i deleted and the integral is taken over $A = (Y_{obs,i}, \infty)^{J-1}$. The term $p(\mathbf{Y}_i | K_i, \mathbf{D}_i, \mathbf{Z}_i, \mathbf{E}_i, \boldsymbol{\theta})$

can be expressed using normal distributions according to the setup for \mathbf{X}_i and Equation (2).

This posterior is analytically intractable, so we adopt Markov chain Monte Carlo (MCMC) techniques for inference. To facilitate computation, we augment the posterior by including the latent variables $\mathbf{Y}_{-obs,i}$, that is, we draw MCMC samples for $\boldsymbol{\theta}$ and $\mathbf{Y}_{-obs,i}$ jointly from

$$p(\boldsymbol{\theta}, \{\mathbf{Y}_{-obs,i}\}_{i=1}^n \mid \{Y_{obs,i}, m_i, K_i, \mathbf{D}_i, \mathbf{Z}_i, \mathbf{E}_i\}_{i=1}^n) \propto \pi(\boldsymbol{\theta}) \prod_{i=1}^n p(\mathbf{Y}_i \mid K_i, \mathbf{D}_i, \mathbf{Z}_i, \mathbf{E}_i, \boldsymbol{\theta}) \cdot I_A(\mathbf{Y}_{-obs,i})$$

where $I_A(\mathbf{Y}_{-obs,i})$ is the usual indicator function that takes value 1 when $\mathbf{Y}_{-obs,i} \in A$. We carry out the required MCMC sampling via Hamiltonian Monte Carlo (HMC) as implemented in Stan (Stan Development Team, 2020).

3 Simulation Study

We first fit our proposed model to simulated data and examine the posterior distributions of the parameters obtained by Bayesian inference. To mimic the subsequent real data analysis, we set $J = 24$, $d_{max} = 96$ (inches), and take $\boldsymbol{\eta} = \{\eta_0, \eta_1\}$ to be the regression coefficients in Equation (1) since each specimen in the real data has one covariate. We also choose values for the model parameters that resemble those found by a preliminary analysis of the real data: $\eta_0 = 3.0$, $\eta_1 = 1.5$, $\rho = 0.7$, $\sigma = 0.8$, $\beta = 0.5$, $\gamma_0 = 0.25$, $\gamma_1 = 0.15$. Then, we simulate datasets of three different sample sizes: $n = 120, 360, 720$ specimens. The standard sample size in lumber testing is 360 specimens (Green and McDonald, 1993), and 120 is close to the sample size of the available data in the present study.

We next detail the steps involved in generating a simulated dataset corresponding to the given parameters and values, independently for each specimen $i = 1, 2, \dots, n$:

1. Generate the covariate $v_i \sim N(1.9, 0.25^2)$. As described in the subsequent real data analysis, this covariate is a measurement of the specimen's overall stiffness, known as the modulus of elasticity (MOE). We treat this as a global covariate common to all J cells. The mean 1.9 and standard deviation 0.25 of the normal distribution are chosen to resemble the empirical distribution of MOE (in units of $\text{psi} \times 10^6$) in the real data.
2. Generate $\mathbf{X}_i \in \mathbb{R}^{J \times 1}$, i.e., the strengths of each cell for a clear specimen, in successive order according to

$$\begin{aligned} X_1 &\sim N(\eta_0 + \eta_1 v_i, \sigma^2 / (1 - \rho^2)) , \\ X_2 &= (1 - \rho)(\eta_0 + \eta_1 v_i) + \rho X_1 + \epsilon_2 , \\ &\vdots \\ X_J &= (1 - \rho)(\eta_0 + \eta_1 v_i) + \rho X_{J-1} + \epsilon_J , \end{aligned} \tag{4}$$

where $\epsilon_2, \dots, \epsilon_J \stackrel{iid}{\sim} N(0, \sigma^2)$. We note that the values of the parameters chosen here all but ensure that the resulting strengths are positive-valued, so the normal distributions can serve as reasonable approximations in practice.

3. Generate the number of knots K_i and locations of the knot centroids \mathbf{S}_i from a homogeneous Poisson point process with constant intensity $\lambda = 0.01$ within the dimensions of the test span (96×5.5 in²). The intensity λ is chosen to resemble the number of knots observed in the real data. We then compute the distance matrix $\mathbf{D}_i \in \mathbb{R}^{J \times K_i}$ given \mathbf{S}_i , and apply the decreasing function $h(\cdot)$ element-wise on \mathbf{D}_i to obtain the weight matrix $\mathbf{W}_i \in \mathbb{R}^{J \times K_i}$.
4. Generate the vector of indicators $\mathbf{E}_i \in \{0, 1\}^{K_i}$ to denote whether each knot is an “edge knot” or not. Each element of \mathbf{E}_i is obtained as an independent Bernoulli(p_e) draw, and the value of $p_e = 0.6$ is chosen based on the observed proportion of edge knots in the real data.
5. Generate the vector of strength-reducing effects $\mathbf{Z}_i \in \mathbb{R}^{K_i \times 1}$. Each element of \mathbf{Z}_i is obtained as an independent draw from a gamma distribution with shape parameter 2.0 and scale parameter 6.0, again informed by the knot volumes extracted from the real data.
6. Calculate $\mathbf{Y}_i \in \mathbb{R}^{J \times 1}$ conditional on the outputs of simulation steps 1–5, using Equation (2). We obtain the observed strength measurement $Y_{obs,i}$ as the minimum of \mathbf{Y}_i and record m_i as the corresponding cell index where failure occurred.

We simulate a dataset for each the three aforementioned sample sizes of specimens (120, 360, and 720). To complete the model specification, we chose weakly informative priors for the parameters as follows:

- $\eta_0 \sim N(0, 10)$, $\eta_1 \sim N(0, 10)$;
- $\rho \sim N(0.5, 0.5^2)$ restricted to $0 < \rho < 1$;
- $\beta \sim N(0, 1)$, $\gamma_0 \sim N(0, 1)$, $\gamma_1 \sim N(0, 1)$, each restricted to the positive half of the standard normal;
- $\sigma \sim Cauchy(0, 5)$.

For each simulated dataset, we fit the proposed model using the methods described in Section 2.2. We ran four parallel chains with 10000 HMC iterations each, and discarded the first 5000 iterations as burn-in. The posterior distributions of the parameters are summarized in Table 1 by displaying their 50%, 2.5%, and 97.5% posterior quantiles. The fits seem reasonable, and it can be seen that the 95% credible intervals (represented by the 2.5% and 97.5% posterior quantiles) all contain the true parameter values shown in the ‘Truth’ column. The widths of these credible intervals also become narrower as the sample size increases. These results indicate that we can expect to obtain useful parameter estimates with a sample size of around 120 specimens, while more precise credible intervals could be obtained with a standard test sample of 360 specimens. The additional precision gained from a further increase to 720 specimens is less pronounced.

Table 1: Summaries of the posterior distributions of the parameters based on simulated datasets with different sample sizes of specimens ($n = 120, 360, 720$). The true parameter values are shown in the ‘Truth’ column. The 50%, 2.5% and 97.5% posterior quantiles are shown for the parameters in each simulated dataset. The 95% credible intervals all contain the true parameter values, and become narrower as the sample size increases.

Parameter	Truth	Posterior quantiles								
		$n = 120$			$n = 360$			$n = 720$		
		50%	2.5%	97.5%	50%	2.5%	97.5%	50%	2.5%	97.5%
η_0	3.00	3.82	2.68	4.96	3.24	2.52	3.97	3.16	2.66	3.66
η_1	1.50	1.12	0.61	1.64	1.30	0.97	1.62	1.46	1.24	1.69
ρ	0.70	0.64	0.26	0.83	0.74	0.61	0.83	0.67	0.56	0.75
σ	0.80	0.83	0.54	1.20	0.71	0.56	0.90	0.86	0.72	1.01
β	0.50	0.48	0.30	0.75	0.49	0.39	0.62	0.52	0.43	0.62
γ_0	0.25	0.23	0.13	0.48	0.24	0.17	0.35	0.26	0.20	0.35
γ_1	0.15	0.13	0.06	0.28	0.13	0.09	0.20	0.15	0.11	0.20

4 Application: Tensile Strength of Douglas Fir

4.1 Tensile Strength Dataset

The modelling approach proposed in this paper is demonstrated on experimental data from a sample of Douglas Fir (DF) lumber specimens. This section describes the procedures we used to collect and process the data.

Preparation of Lumber Specimens

The lumber specimens were prepared and tested in the wood products testing laboratory of FPIInnovations located in Vancouver, Canada. The wood species of the specimens in our study was DF, which is widely used for making sawn lumber thanks to its strong and stable wood quality (Vikram et al., 2011). Our DF specimens were 12-ft long nominal 2 by 6 boards (actual dimensions $1.5'' \times 5.5'' \times 12'$). A visual examination of the specimens indicated that the lumber was of high quality, with the number of knots per specimen ranging from zero to eight (only knots of meaningful size are counted, i.e., 1/10th of the specimen width or larger). A total of 113 specimens were available for this study.

To photograph the lumber surfaces, each specimen was fed through a scanner equipped with rollers and two sets of digital cameras; a diagram of the setup is shown in the Appendix of Pan et al. (2021). The knot faces on the photographs were then identified and annotated with the assistance of a team of undergraduate students. Next, the knot matching algorithm of Jun et al. (2019) was run to determine the most likely correspondence between knot faces and tree branches. The 3-D structure of a knot was then reconstructed as the convex hull containing its knot faces that were matched together, from which the volume displaced by the knot could be calculated. Finally, the stiffness (MOE) of each specimen was measured via the transverse vibration method.

Lumber Strength Testing

The tensile test machine, which meets the requirements of ASTM Standard Test Method D4761 (ASTM International, 2019), operates by pulling longitudinally on the two ends specimen; a schematic is shown in Figure 2. The machine has clamps that grip the specimen firmly at its two ends using a grip length of 2-ft, so with 12-ft specimens this results in an 8-ft test span between the grips. The grip is set so as to ensure that the tensile forces are axial can be assumed to be uniform along the specimen length between the inside edges of the grips. After the test begins, the tensile load applied (in lbs) is increased linearly at a constant rate and monitored via two load cells. The test is destructive in that all specimens are loaded until failure; the rate is set such that the average time taken to break a specimen is approximately 1 minute. The ultimate tensile strength (UTS) is calculated from the maximum load applied to the specimen immediately before it breaks, by converting to the equivalent pounds per square inch (psi).

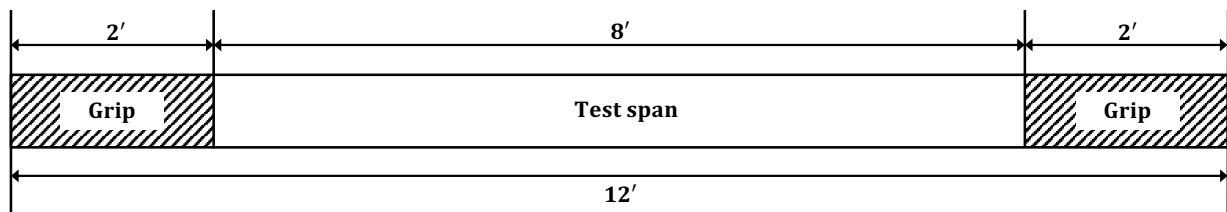


Figure 2: Schematic diagram of the tensile strength test setup. Note the 8-foot test span between the grips at each end.

After the tensile test is complete, the location of failure on the specimen must be determined by visual examination; this is defined by the location where the specimen first begins to fracture. Due to the setup of the grips, the failure location will be a longitudinal position between 24" and 120" from one end of the specimen. There is often some uncertainty in determining the exact location, because a fracture can be several inches long. Thus, we chose the cell size in the modelling framework (Section 2.1) as 4", to correspond with the resolution at which most failure locations can be determined confidently. This leads to taking $J = 24$ as the number of cells for representing the 8-ft test span between the grips, and recording the failure location for each specimen as the cell index (1–24).

The measurements described in this section are summarized for the 113 specimens via the histograms in Figure 3. The panels depict histograms of the MOE ($\text{psi} \times 10^6$), UTS ($\text{psi} \times 10^3$), and the cell indices of the failure locations (1–24). The empirical distributions of MOE and UTS are approximately symmetric, with UTS having a slight right skew. It can also be seen that the cell indices recorded for the failure locations in our sample are distributed relatively uniformly across the test span.

4.2 Model fitting results

We fit the proposed model to the knot and tensile strength experimental data described in Section 4.1, where we set $J = 24$ and $d_{max} = 96\text{in}$ to correspond to the length of the test span. Since the MOE is measured for each specimen as a whole, we treat it as a global covariate that is common to all J cells of a specimen and take $\boldsymbol{\eta} = \{\eta_0, \eta_1\}$ to be the regression coefficients in Equation (1); i.e., as in the simulation study (Section 3) we have

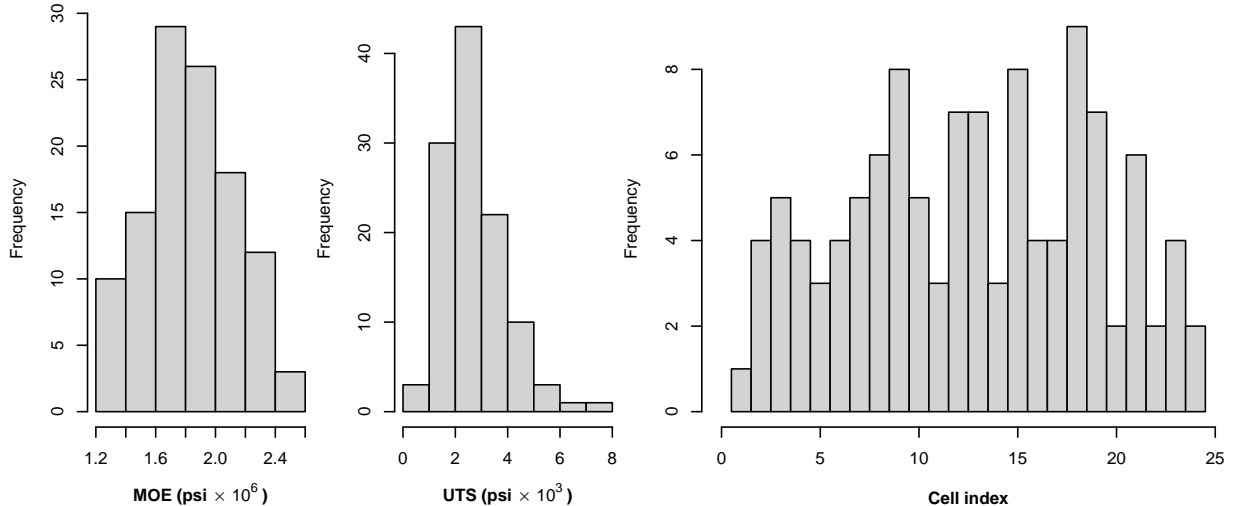


Figure 3: Histograms of the MOE ($\text{psi} \times 10^6$), UTS ($\text{psi} \times 10^3$), and the cell indices of the failure locations (1–24), for the sample of 113 Douglas Fir specimens used in this study.

for an individual specimen $\boldsymbol{\eta}^T \mathbf{v}_j = \eta_0 + \eta_1 \cdot \text{MOE}$, $j = 1, \dots, 24$. We also adopt the same priors as introduced in the simulation study.

We ran four parallel chains with 10000 HMC iterations each, and discarded the first 5000 iterations as burn-in. Convergence was observed in the trace plots, and summaries of the posterior distributions for the parameters are reported in Table 2. The widths of the 95% credible intervals (represented by the 2.5% and 97.5% quantiles) are comparable to those from the 120 specimen simulation study in Table 1.

Table 2: Summary of the posterior distributions of the parameters, based on fitting the model to the Douglas Fir experimental data. The 50%, 2.5%, and 97.5% posterior quantiles are shown for each parameter.

Parameter	Posterior quantiles		
	50%	2.5%	97.5%
η_0	2.59	1.20	4.03
η_1	1.69	1.05	2.33
ρ	0.76	0.52	0.88
σ	0.94	0.61	1.44
β	0.40	0.25	0.64
γ_0	0.30	0.18	0.55
γ_1	0.12	0.07	0.23

4.3 Predicting the Tensile Strength of Lumber

The fitted Bayesian model provides a posterior predictive distribution for lumber tensile strength, given the MOE and spatial arrangement of knots (i.e., as represented via $\mathbf{W}_i, \mathbf{Z}_i, \mathbf{E}_i$ in the modelling framework) for a new specimen. An estimate of this predictive strength distribution is obtained by taking each MCMC draw of the parameters, using

Equation (4) to generate \mathbf{X}_i , then using Equation (2) to generate \mathbf{Y}_i and setting $\min\{\mathbf{Y}_i\}$ to be the tensile strength.

To assess the efficacy of our modelling approach, we performed five-fold cross-validation to evaluate predictive performance. To provide a baseline for comparison, we consider our Bayesian model along with two basic regression models for UTS:

$$\text{Regression Model 1 : UTS} = \beta_0 + \beta_1 \cdot \text{MOE} + \epsilon ,$$

$$\text{Regression Model 2 : UTS} = \tilde{\beta}_0 + \tilde{\beta}_1 \cdot \text{MOE} + \tilde{\beta}_2 \cdot \max(\mathbf{Z}_i) + \tilde{\epsilon} .$$

The first model only uses the MOE as a predictor, while the second model also includes the worst individual knot effect, defined via $\max(\mathbf{Z}_i)$ in our notation. Inclusion of the worst knot mimics the setup of some previous regression models for lumber strength (as described in the Introduction, e.g., Divos and Tanaka, 1997).

For our Bayesian model, we treat the mean of the posterior predictive distribution as the predicted strength for the validation specimens, and consider the 2.5% and 97.5% quantiles as a 95% prediction interval. The cross-validated prediction results are summarized for the three models in Table 3. The mean predicted tensile strength for each model over the 113 specimens is close to the empirical mean UTS in the dataset of 2.72, which indicates that our Bayesian predictions have little or no bias in practice. As metrics to evaluate the predictive performance of each model, we compute the mean-squared prediction error (MSPE), mean absolute prediction error (MAPE), and mean length of the 95% prediction intervals. Including the worst knot in the basic regression model leads to a marked improvement in MSPE compared to a regression on MOE alone (1.04 vs. 1.23), and our proposed Bayesian model that accounts for the entire spatial arrangement of knots yields a modest further improvement (MSPE = 0.96). A similar pattern is seen when considering MAPE. Finally, the Bayesian model also provides the narrowest 95% prediction intervals on average. These results confirm the importance of knots and their spatial arrangement in lumber strength prediction.

Table 3: Summary metrics for the predictive performance of two linear regression models and the proposed Bayesian model, by applying five-fold cross-validation on the Douglas Fir dataset. The mean tensile strength in the dataset is 2.72 and close to the mean predictions given by the three models under cross-validation. The mean-squared prediction error, mean absolute prediction error, and mean length of 95% prediction interval are computed for each model.

Metric	Model		
	Regression 1	Regression 2	Bayesian spatial
Mean prediction	2.71	2.71	2.73
Mean-squared prediction error	1.23	1.04	0.96
Mean absolute prediction error	0.88	0.80	0.78
Mean length of 95% prediction interval	4.37	4.06	3.94

5 Discussion and conclusions

This paper proposed a new approach for modelling the tensile strength of lumber, based on the spatial arrangement of knots extracted from the surface scans of specimens. In

particular, the resulting model accounts for the locations and strength-reducing impacts of all relevant knots, as derived from reconstructing their 3-D volumes. Furthermore, any other non-destructive measurements taken on the specimen, such as MOE, could be incorporated in the modelling framework as local or global covariates. The usefulness of our approach is demonstrated via simulation studies and a real data analysis based on a sample of 113 DF specimens, which showed that our proposed method outperforms the basic regression models on predictive performance.

A goal of this study was a proof-of-concept for our strength prediction approach, which we believe has been achieved. Its scientific value lies in showing how different knots on a lumber specimen work together to reduce its strength. By conceptually partitioning a specimen into cells, our fitted model helps provide insight into a knot's effect as a function of distance. The posterior distribution of the model parameter β suggests that the spatial effect of a knot decays at a rate of approximately $e^{-0.40d}$, where d denotes the distance (in inches) between the knot location and a cell centroid. (Note that the quantity 0.40 has units in^{-1} so that the exponential is unitless.) Moreover, the fitted model sheds light into the effect of a knot's location, via the parameters γ_0 and γ_1 that scale a knot's strength reduction depending on whether it is situated on the edge of a specimen. Based on the 113 specimens available, the 95% credible intervals were (0.18, 0.55) for an edge knot and (0.07, 0.23) otherwise. This suggests it is likely that their effects are different, especially if a larger sample of specimens were to be tested to yield more precise credible intervals. In contrast, a previous experiment that recorded only the information of the worst knot on each specimen failed to find evidence of knot location having an impact on UTS (Wong et al., 2016). Overall, our approach recognizes and demonstrates the value of analyzing complete information on the spatial arrangement of knots.

The metrics for predictive performance presented in Section 4.3 showed that our Bayesian model achieved the lowest MSPEs, lowest MAPEs, and shortest 95% prediction intervals compared with two other regression models. All three models included MOE, which is recognized to be a strong predictor of UTS and other strength properties of lumber, for example as used in monitoring programs (Kretschmann et al., 1999). Adding the effect of the worst knot improved predictions, and using the complete spatial arrangement of knots in our Bayesian model yielded further improvements, albeit modest. Our relatively minor gains may be due in part to limitations of the available sample of specimens for this study. The Bayesian model is more complex relative to the amount of information contained in this small sample of lumber, and we would expect to see more substantial gains in samples of the size more commonly seen in lumber testing of over 300 pieces (see for example, ASTM International (2007), Note 7). Also, the high grade quality of the DF specimens is less ideal for studying the effects of knots, as the number of knots per specimen was relatively low (average 3.8) and limited the information available for learning knot parameters.

As practical implications of this study, our proof-of-concept shows that more extensive testing and efficient scanning techniques would be desirable, to produce larger samples representing more diverse lumber populations (e.g., different species and dimensional sizes). In particular, an interesting extension would be to take multiple strength measurements on a single specimen, to better understand how strength varies along a piece of lumber. We note that even modest gains in strength prediction accuracy would be worthwhile, with the large volumes of lumber being produced worldwide and the increasing popularity of wood as a sustainable building material. More accurate predictions could in turn reduce the within-grade strength variation, via updates to the rules used to classify lumber into

grades. This would be beneficial for both manufacturers and consumers of lumber, in terms of extracting better value from harvested trees and meeting strength requirements for intended uses with greater confidence. Overall, the model and approach presented could lead to a more refined way of managing the quality of manufactured lumber.

Acknowledgements

The work reported in this paper was partially funded by FPInnovations and grants from the Natural Science and Engineering Research Council of Canada. The authors thank Conroy Lum, along with FPInnovations and its technical support staff, for facilitating the experimental work that was done to produce the data used in this paper. Thanks also to Conroy for helping the authors understand better the complexities involved in grading lumber. As well the work profited from the comments of members of the Forest Products Stochastic Modelling Group, centered at the University of British Columbia.

References

- ASTM International (2007). D1990-07: Standard practice for establishing allowable properties for visually-graded dimension lumber from in-grade tests of full-size specimens.
- ASTM International (2019). D4761-19: Standard Test Methods for Mechanical Properties of Lumber and Wood-Base Structural Material.
- Canadian Lumber Standards Accreditation Board (2021). Lumber grades. <https://www.clsab.ca/faq-items/how-were-the-design-values-established-for-structural-lumber/>. Accessed 02/26/2022.
- Castéra, P., Faye, C., and El Ouadrani, A. (1996). Prevision of the bending strength of timber with a multivariate statistical approach. *Annals of Forest Science*, 53(4):885–896.
- Courchene, T., Lam, F., and Barrett, J. (1998). The effect of edge knots on the strength of SPF MSR lumber. *Forest products journal*, 48(4):75.
- Cramer, S. and Goodman, J. (1983). Model for stress analysis and strength prediction of lumber. *Wood and Fiber Science*, 15(4):338–349.
- Divos, F. and Tanaka, T. (1997). Lumber strength estimation by multiple regression. *Holzforschung*, 51(5):467–471.
- Fink, G. and Kohler, J. (2014). Model for the prediction of the tensile strength and tensile stiffness of knot clusters within structural timber. *European Journal of Wood and Wood Products*, 72(3):331–341.
- Foley, C. (2003). *Modeling the Effects of Knots in Structural Timber*. PhD thesis, Lund University, Sweden.
- França, F., Seale, R. D., Shmulsky, R., and França, T. (2018). Modeling mechanical properties of 2 by 4 and 2 by 6 southern pine lumber using longitudinal vibration and visual characteristics. *Forest Products Journal*, 68(3):286–294.

- García, D. A. and Rosales, M. B. (2017). Deflections in sawn timber beams with stochastic properties. *European Journal of Wood and Wood Products*, 75(5):683–699.
- Green, D. W. and McDonald, K. A. (1993). Investigation of the mechanical properties of red oak 2 by 4's. *Wood and fiber science*, 25(1):35–45.
- Harte, A. M. (2017). Mass timber—the emergence of a modern construction material. *Journal of Structural Integrity and Maintenance*, 2(3):121–132.
- Hietaniemi, R. and Silvén, O. (2011). Camera based lumber strength classification system. In *MVA2011 IAPR Conference on Machine Vision Applications*, pages 251–254.
- Jun, S.-H., Wong, S. W., Zidek, J. V., and Bouchard-Côté, A. (2019). Sequential decision model for inference and prediction on nonuniform hypergraphs with application to knot matching from computational forestry. *The Annals of Applied Statistics*, 13(3):1678–1707.
- Kandler, G., Füssl, J., and Eberhardsteiner, J. (2015). Stochastic finite element approaches for wood-based products: theoretical framework and review of methods. *Wood science and technology*, 49(5):1055–1097.
- Kretschmann, D. E., Evans, J. W., and Brown, L. (1999). *Monitoring of visually graded structural lumber*, volume 576. US Department of Agriculture, Forest Service, Forest Products Laboratory.
- Lukacevic, M., Füssl, J., and Eberhardsteiner, J. (2015). Discussion of common and new indicating properties for the strength grading of wooden boards. *Wood Science and Technology*, 49(3):551–576.
- Oh, J.-K., Kim, K.-M., and Lee, J.-J. (2010). Use of adjacent knot data in predicting bending strength of dimension lumber by x-ray. *Wood and fiber science*, 42(1):10–20.
- Pan, S., Fan, S., Wong, S. W., Zidek, J. V., and Rhodin, H. (2021). Ellipse detection and localization with applications to knots in sawn lumber images. In *Proceedings of the IEEE/CVF Winter Conference on Applications of Computer Vision*, pages 3892–3901.
- Reynolds, R. V. R. and Pierson, A. H. (1923). *Lumber Cut of the United States, 1870-1920*. Number 1119. US Department of Agriculture.
- Stan Development Team (2020). RStan: the R interface to Stan. *R package version 2.21.2*.
- Taylor, S., Bender, D., Kline, D., and Kline, K. (1992). Comparing length effect models for lumber tensile strength. *Forest products journal*, 42(2):23–30.
- Tegel, W., Elburg, R., Hakelberg, D., Stäuble, H., and Büntgen, U. (2012). Early neolithic water wells reveal the world's oldest wood architecture. *PloS one*, 7(12):e51374.
- Vikram, V., Cherry, M. L., Briggs, D., Cress, D. W., Evans, R., and Howe, G. T. (2011). Stiffness of douglas-fir lumber: effects of wood properties and genetics. *Canadian Journal of Forest Research*, 41(6):1160–1173.

- Wong, S. W., Lum, C., Wu, L., and Zidek, J. V. (2016). Quantifying uncertainty in lumber grading and strength prediction: a Bayesian approach. *Technometrics*, 58(2):236–243.
- Zidek, J. V. and Lum, C. (2018). Statistical challenges in assessing the engineering properties of forest products. *Annual Review of Statistics and Its Application*, 5:237–264.